Theoretical insight into effect of cation–anion pairs on CO_2 reduction on bismuth electrocatalysts

Sun Hee Yoon[a,1], Guangxia Piao[b,1], Hyunwoong Park[b,*], Nimir O. Elbashir[c,d], Dong Suk Han[e,*]

[a] Petroleum Engineering Program, Texas A&M University at Qatar, Doha 23874, Qatar
[b] School of Energy Engineering, Kyungpook National University, Daegu 41566, Republic of Korea
[c] Petroleum Engineering and Chemical Engineering Programs, Texas A&M University at Qatar, Doha 23874, Qatar
[d] TEES Gas & Fuels Research Center, Texas A&M University, College Station, TX 77843, USA
[e] Center for Advanced Materials (CAM), Qatar University, Doha 2713, Qatar

ARTICLE INFO

ABSTRACT

This study presents theoretical insight into the mechanism of the CO_2 reduction reaction (CO_2RR) to formic acid (HCOOH) on Bi (0 1 2) surfaces in the presence of alkali metal cations (M^+: Cs^+, K^+, and Li^+) and/or halide anions (X^-: Cl^-, Br^-, and I^-) using density functional theory (DFT). The adsorption energy (E_{ads}) and work function (W_f) of the anions increases with decreasing anion size (i.e., $Cl^- > Br^- > I^-$). On the other hand, the larger the cation size is, the higher is the E_{ads} (i.e., $Li^+ < K^+ < Cs^+$) but the lower is the W_f (i.e., $Cs^+ < K^+ < Li^+$). In the presence of the cation–anion pairs (M^+/X^-), E_{ads} of the pairs on hydrated Bi (Bi-2H) becomes more negative than that in the cases of anions or cations alone, particularly when the ionic radius of the paired cation and anion do not differ significantly. Such a synergistic effect of the mixed ions is also observed for the work function values. In the case of anions alone, CO_2 molecules prefer to coordinate directly with hydrated Bi atoms via the oxygen bidentate mode; in the case of cations alone, CO_2 molecules directly bind to the cations via the oxygen monodentate mode, rather than the hydrated Bi atoms. Between two possible CO_2RR pathways involving *OCHO and *COOH intermediates on Bi-2H pre-adsorbed with M^+/X^-, the former pathway requires less energy for all M^+/X^- pairs. In addition, cascaded reaction profiles from CO_2* to HCOOH are obtained with Cs^+/Cl^- and K^+/Cl^- pairs in the former. This indicates that once CO_2 is adsorbed, the following reactions proceed spontaneously on Bi-2H with Cs^+/Cl^- or K^+/Cl^- pairs. This study thus shed light on the positive effects of supporting electrolytes (e.g., CsCl and KCl) on catalytic CO_2RR.

1. Introduction

Electrochemical CO_2 reduction reaction (CO_2RR) has been demonstrated to be an efficient method to convert CO_2 into value-added chemicals such as formic acid (FA) [1], CO [2], methanol [3], and ethylene [4]. The faradaic efficiency and selectivity of CO_2RR is improving, but the practical application of the system on a large scale is still limited due to the large overpotentials and low durability of the electrocatalysts involved [3,5]. To overcome these challenges, significant efforts have been directed toward synthesizing efficient, durable, and inexpensive electrocatalysts [2,6–11]. Among them, bismuth-based materials are considered suitable due to their operation with high selectivity of FA and durability in aqueous potassium bicarbonate solutions [2,11]. Interestingly, the use of an ionic liquid (e.g., 1,3-dialkyl-substituted imidazolium) enhanced the interaction of CO_2 with the Bi

surface, shifting the equilibrium of the reaction toward CO production [12]. This suggests that the selectivity of Bi materials largely depends on the type of supporting ion and/or size of the ions in the solution [13–15].

Such an effect of the electrolyte on the selectivity of CO_2RR does not necessarily hold true for other catalyst materials. For example, Ag became more selective for CO production when Li^+ was replaced with a larger ion, Cs^+ [16]. In contrast, Cu-based catalysts led to similar ratios of C_2H_6/H_2 in aqueous electrolytes when using Li^+ and Cs^+ [15]. The effect of halide anions on the selectivity is also dependent on the type of materials used. Cl^- has been noted to enhance the selectivity of CO production with Ag [15,17] and Au [18], whereas I^- exerted the greatest effect on the CO production on Cu followed by Br^- and Cl^- [19,20]. On the other hand, for Bi electrodes, halide anions (X^-) and alkali metal cations (M^+) significantly influenced the selectivity of FA

---

by enhancing the charge transfer ($Cl^- > Br^- \sim I^-$) and increasing the local CO_2 concentration ($Cs^+ > K^+ > Li^+$) [2,15]. Despite these observations, the reason behind the type of ions changing the selectivity remains unclarified in terms of the mechanism involved. This is partly attributed to the fact that the interactive influence of certain ions and their counter ions (i.e., cations and anions) on the charge transfer of CO_2RR can be significantly altered simply by changing either the ions or the counter ions. So far, mixed types of cations–anion combinations (M^+/X^-) have not been sufficiently studied in terms of their structures and behaviors, as most theoretical and experimental studies on the effect of ions have focused on the role of only one type of cations or anions (M^+ or X^-).

With this in mind, we employed DFT calculations to gain theoretical insight into the selective CO_2RR in various electrolytes using Bi (012) as a model electrocatalyst since the (012) plane was found to be the highest intensity in X-ray diffraction experiments [21]. Prior to studying the selectivity, we first examined the structural and electrical properties occurring in the interface between Bi and the single or mixed types of ions. Then, DFT calculations were performed to identify the activities of cations alone or anions alone, as well as mixed types of ions on hydrated Bi (i.e., Bi-2H). In particular, the possible reaction pathways from CO_2 to FA were explored through *OCHO or COOH* intermediates in the proton-coupled electron transfer processes on the hydrated Bi with those ions. A previous work focused on the CO_2RR pathways with monatomic ions [22], but this study further advances the existing knowledge in the field by highlighting the effect of mixed types of ions on the CO_2RR pathways and products.

2. Computational methodology

2.1. Method and model construction

All the calculations in this study were performed using density functional theory (DFT) implemented in the Atomistix ToolKit-Virtual NanoLab package [2]. To describe the electronic interactions in bismuth, the exchange–correlation functional of Perdew, Burke, and Ernzerhof (PBE) within the generalized gradient approximation (GGA) was applied. Grimme DFT-D2 correction was adopted to allow for van der Waals interactions between the CO_2 molecule and Bi, or between the CO_2 molecule and adsorbates (single and mixed types of ions). The PBE + D2 methodology predicted the phase stability of ions adsorbed on the Bi (012) surface [21]. The bulk unit cell structure of Bi mentioned in Table S1 was optimized to determine the equilibrium lattice structure, which was then cleaved into a slab model to describe the surface orientation of Bi. The slab model supercell was constructed in repetitions (2 × 1 × 1) with a 15 Å vacuum layer to prevent interactions between artificial inter-slabs. For geometry optimization, 3 × 3 × 1 k-point samplings were performed. Of the total five layers, three lower layers were fixed, while the two upper layers adsorbing all species were allowed to relax at the force tolerance of 0.05 eV Å^{-1} for optimization. We assumed in the same way as previous papers dealing with metal catalysts that attempted surface chemistry with the slab model [14,23]. Also, Mavrikakis et al. and Izzaouihda et al. investigated a correlation between adsorption energy of adsorbates and a number of pure metal layers. They concluded that the adsorption energy of small adsorbate molecules was not affected by over two metal layers [24,25]. Based on this result, we considered the stability between an adsorbate and the Bi slab surface and the fixed bottom layers for the remaining bulk below the surface. Adsorption sites for adsorbates were considered from the initial guesses of the adsorption structures by inferring the binding geometry and adsorption potential sites in an arbitrary pattern. This approach focused on the adsorption state of CO_2 and ions on the high- index plane (012) of Bi found in previous experiments [2]. Then, DFT calculations were performed to find the most stable adsorption sites by relaxing the atomic positions until a total residual force was less than 0.05 eVÅ^{-1}. Based on the reaction pathways of the CO_2 molecule,

*OCOH, *COOH, and *HCOOH species are adsorbed on the top layer of Bi-2H and HCOOH is present as a species from desorbed the Bi-2H surface. The transition state through the reaction pathway was confirmed by DynamicMatrix of the Nudge Elastic Band (NEB). The asterisk (*) denotes the state of being adsorbed on the Bi surface.

2.2. Electrical properties and reaction energies

To investigate the thermodynamic stability of adsorbates on clean Bi and Bi-2H surfaces, we computed the adsorption energy (E_{ads}) as follows:

$$E_{ads} = E_{(ions-slab)} - E_{(slab)} - E_{(ions)} \qquad (1)$$

where $E_{(ad-slab)}$, $E_{(slab)}$, and $E_{(ad)}$ are the total energies of ions on the clean Bi slab, the total energy of the slab, and the total energy of an isolated type of ions, respectively. Herein, the ions represent one type (M^+ or X^-) and mixed types (M^+/X^-) of ions adsorbed on Bi. The single types of ions consist of an atom and the cation–cation mixed types are defined as two atoms in total: one alkali metal atom and one halide atom. The Bi-2H structure refers to H^+ species adsorbed onto a clean Bi surface mediated by water. The adsorption energy of clean Bi was compared with that of Bi-2H. The adsorption energy of CO_2 (E_{ads_CO2}) was calculated as follows.

$$E_{ads\_CO2} = E_{(CO2/ions-slab)} - E_{(ions-slab)} - E_{(CO2)} \qquad (2)$$

where $E_{(CO2/ions-slab)}$, $E_{(ions-slab)}$, and $E_{(CO2)}$ are the total energies of a CO_2 molecule (adsorbed on Bi with the ions), Bi with the ions, and an isolated CO_2 molecule, respectively. All calculations for the adsorption energy were carried out for one side of the slab. In addition, the work function (W_f) was calculated to quantify the minimum thermodynamic energy required to remove electrons from the Bi catalyst to CO_2 (Eq. (3)).

$$W_f = -e\emptyset - E_f \qquad (3)$$

where e is a charge of an electron, $\emptyset$ is the electrostatic potential in the vacuum near the Bi surface, and E_f is the Fermi level inside the Bi metal [26]. To observe the distribution of charges between adsorbates (i.e., ions and CO_2) on Bi through the assigned cell structure, the charge transfer, the electron density of the isolated system (adsorbates), and the electrical potential of the bulk system (all adsorbates + Bi crystal structure) were calculated. To account for the charge transfer, Bader charge analysis was performed at all electron densities. The electrostatic potential was obtained through the Poisson solver, in which the boundary condition for the bulk systems was periodic [27]. The computational hydrogen electrode (CHE) model described by Nørscov et al. [28] was used to establish a free energy pathway in the chemical potential of proton–electron pairs, i.e., $\mu(H^+ + e^-)$. The chemical potential (μ) in the model is equal to $1/2[(\mu(H_2(g))]$ which means a half of the hydrogen in the gas phase at 0 V (reversible hydrogen electrode, RHE) for any pH. Based on the total chemical potential of a proton–electron pair, a potential-dependent reaction free energy ($\Delta G_{i \to j}$ (U)) generated by the electrochemical CO_2RR at an electrode potential (V vs. RHE) can be expressed as follows [29,30].

$$\Delta G_{i \to j}(U) = \Delta G_j(U = 0) - \Delta G_i(U = 0) + eU \qquad (4)$$

where G is the free energy for the individual species (i, j) generated sequentially according to the electrochemical CO_2 reduction step. In previous studies, the contributions to free energies of CO_2 molecule and its intermediates were obtained from the zero-point energy (ZPE)-corrections and entropies [31]. The ZPE-corrections were obtained by calculating vibrational frequency [21,32]. e and U in the chemical potential of the electron (eU) are the elementary charge and electrode potential (V vs. RHE), respectively. To clarify the role of single and mixed types of ions on Bi on the selectivity of CO_2 reduction products, the solvation corrections of water effect was implicitly considered. As a key parameter accounting for the solvation, the dielectric constant
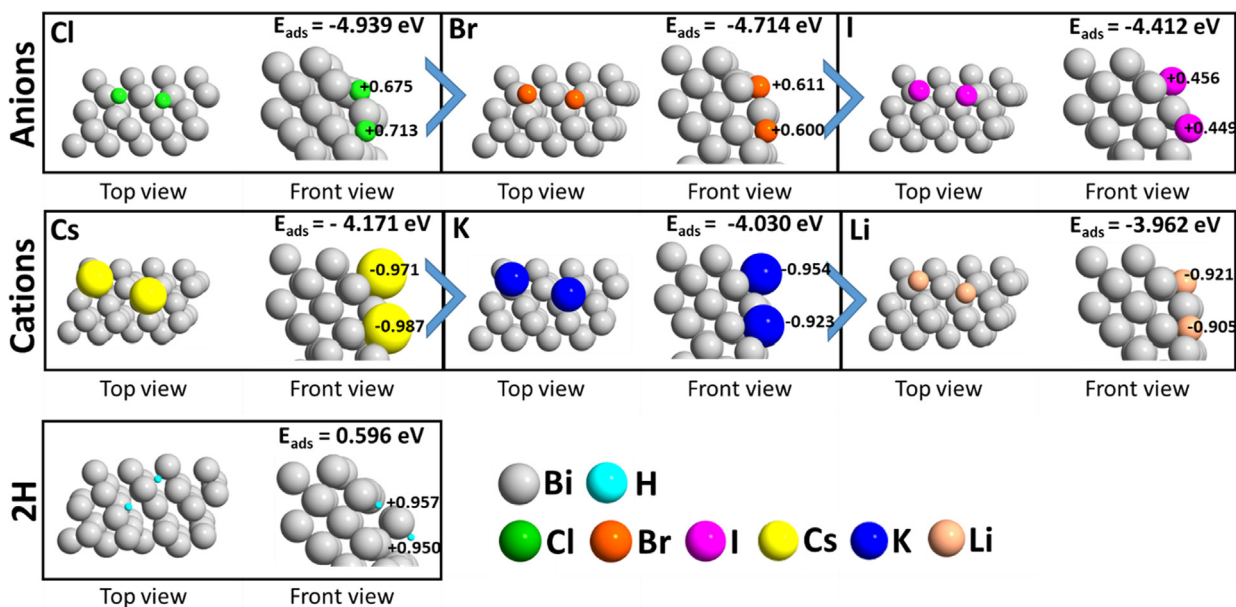
Fig. 1. Illustration of optimized structures and **Bader charge analysis** for ionic radii and adsorption energies of covalent atoms ($2Cl^-$, $2Br^-$, $2I^-$, $2Cs^+$, $2K^+$, $2Li^+$) and $2H^+$ adsorbed on the top site of clean Bi (0 1 2). The geometric structures of ions are induced by adsorption on the top site of clean Bi with 2/9 surface coverage. **Bader charges represent in a unit of |e|.**
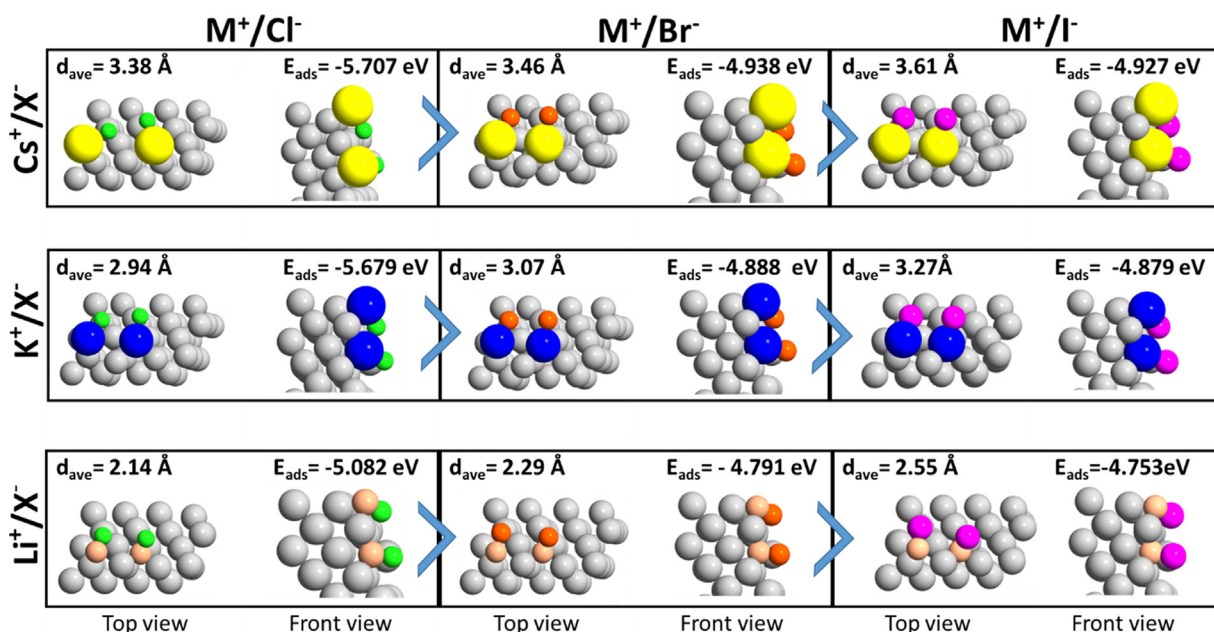
Fig. 2. Illustration of optimized structures and adsorption energies of mixed ions (M^+/X^-) adsorbed on the top site of clean Bi (0 1 2). The geometric structures of the mixed ions are initiated by adsorption on the top site of clean Bi with 2/9 surface coverage. M^+ and X^- denote alkali metals cations and halide anions, respectively.

function of the implicit solvent was set at 80 [33].

3. Results and discussion

3.1. Structural stability for single and mixed types of ions adsorbed on clean Bi surface

The interaction between ions and Bi (0 1 2) surface plays a crucial role in determining the interfacial reaction and catalytic efficiency. To understand the interaction, the adsorption behaviors of single (M^+ or X^-) and mixed types (M^+/X^-) of ions on the surface of Bi were studied. Fig. 1 shows the optimized geometry and adsorption energy (E_{ads})

of the single types of ions and H^+ adsorbed on the clean Bi. When the geometry was optimized, the adsorption sites of all three halide anions and the Li^+ cation changed from the top of Bi to the hollow sites, making the structure more stable. The other two cations (Cs^+ and K^+) were more strongly adsorbed at the bridge site. The preferential ion adsorption sites on the clean Bi are consistent with the results obtained for some other metals (Ag and Cu) in a previous study employing the HF/BLYP method [2]. The adsorption energy of all the ions (except for H^+) was estimated to be negative ($E_{ads} < 0$), suggesting that the ion adsorption occurs spontaneously regardless of the types of ions. Notably, the adsorption energy of the anions became more negative (i.e., $Cl^- > Br^- > I^-$) with decreasing their size (0.181, 0.196, and

0.220 nm for Cl^-, Br^-, and I^-, respectively), whereas a larger cation (0.069, 0.138, and 0.170 nm for Li^+, K^+, and Cs^+ respectively) showed a more negative adsorption energy (i.e., Cs^+ > K^+ > Li^+) [34]. This tendency for the adsorption energy depending on the type and size of ions is similar to that noted previously [35]. Another notable point is that Bader charge analysis shows the opposite trend of E_{ads} and W_f of cations and anions. As shown in Fig. 1, the charges for the adsorbed anions have a positive value. More electron exchange between Cl ions and Bi atoms means a small work function that can easily provide electrons. It can also be seen that active electron exchange is strongly adsorbed with Bi atoms. For adsorbed cations, it shows a negative charge, as opposed to an anion. The cations showed more electron transfer with Bi atoms and could promote CO_2 reduction as a more active electron donor. On the other hand, the adsorption energy of two H^+ atoms on the top site of clean Bi was calculated to be +0.596 eV, indicating that some external potential is necessary for inducing H^+ adsorption.

The adsorption sites and energies of cation–anion pairs (M^+/X^-) adsorbed on the clean Bi surface were also examined (Fig. 2). During the optimization process for the geometrical structure, Cs^+/X^- and K^+/X^- pairs were bound to the bridge and hollow sites of clean Bi, whereas L^+/X^- pairs tended to be adsorbed to the hollow site only. It is noteworthy that the average bond length (d_{ave}) of the ion pairs are comparable to the ionic bond lengths of the respective ionic crystals. More importantly, the pairs with a small anion for the same cation and a large cation for the same anion bind more strongly. This indicates that when the paired cation and anion bind more closely, they have a high adsorption energy, resulting in structural and energy stability.

3.2. Adsorption energy vs. work function for CO_2 adsorption on hydrated Bi surface

The adsorption energy and work function of single and mixed types of ions for hydrated Bi surface (Bi-2H) was examined in the absence and presence of CO_2 adsorption (Table S2). Generally, the adsorption energy serves as an indicator to determine thermodynamic properties of the metal surface and the work function is a descriptor of the adsorption energy [36]. In this study, the adsorption energy indicates whether the Bi-2H surface is stable, depending on how strongly the Bi atoms binds to the ions. The value of the work function is the magnitude of energy indicating whether the stabilized Bi-2H surface can readily provide electrons to interfacial electron acceptors (e.g., CO_2). The ion adsorption on the Bi-2H surface can change the work function (W_f) of the Bi due to the interfacial electrons.

The adsorption energy of halide ions adsorbed to the bridge site of Bi-2H increased in the same order (Fig. 3a) as that noted for clean Bi: Cl^- > Br^- > I^-. This trend for the E_{ads} of halide ions is consistent with previous reports on Hg [37]. The W_f value of Bi-2H was found to increase as the adsorption energy of halide ions increased (Cl^- ~ Br^- > I^-). The work function and adsorption energy of anions were inversely proportional to their size. This suggests that a strong adsorption of anion makes electron transfer from the Bi-2H to an interfacial acceptor (i.e., CO_2) more difficult. On the other hand, alkali metal cations were preferentially bound to the top and bridge sites of the Bi-2H, with the adsorption energy following the order Li^+ < K^+ < Cs^+. However, opposite results for alkali metal cations have been reported elsewhere [36], due to the consideration of different adsorption sites in this study. It should be noted that the magnitude of the E_{ads} for the alkali metal cations can vary, particularly depending on the adsorption sites. For example, E_{ads} of K^+ was more negative than that of Li^+ at the top and bridge sites of a pristine graphene, but the opposite result was found at the hollow sites [38]. Meanwhile, the W_f was inversely proportional to the adsorption energy of alkali metal ions: Cs^+ < K^+ < Li^+. The relationship between E_{ads} and W_f is the opposite of that for halide anions; the larger the cation is, the higher is the adsorption energy, but the smaller is the work function. This suggests that Bi-2H activated by Cs^+ cation requires a minimal thermodynamic energy to transfer electrons to CO_2^*, providing more stable sites to react with CO_2.

The adsorption energy of CO_2 onto Bi-2H pre-adsorbed with halide anions decreased with decreasing anion size (Fig. 3b). Hence, the Bi surface with Cl^- is most favored for CO_2 adsorption, whereas the largest thermodynamic energy is required for the interfacial electron transfer to the adsorbed CO_2 on the Bi with Cl^- due to the largest W_f value. Among the cations, Cs^+ was found to be the best for CO_2 adsorption while minimizing W_f, followed by K^+ and Li^+. In contrast to the case of halide anions, the cation size plays a positive role in the CO_2 adsorption and following interfacial charge transfer.

The optimized adsorption geometries of CO_2 on the Bi-2H pre-adsorbed with anions or cations is shown in Fig. S1. The CO_2 adsorption led to rearrangement of the pre-adsorbed ions from the bridge site to the top site of the Bi-2H, where each ion covered 2/9 of the surface. Two adsorption modes of CO_2 were found: the oxygen bidentate mode for anions and oxygen monodentate mode for cations. The oxygen monodentate and bidentate modes represent that one and two O atoms of adsorbed CO_2 (i.e., CO_2^*) are coordinated with the Bi surface, respectively [38]. In the case of anions, CO_2 molecules prefer to coordinate directly with Bi atoms; in the case of cations, CO_2 molecules directly bind to the cations rather than the Bi atoms. Accordingly, electron transfer can occur directly in the presence of anions (i.e., Bi →
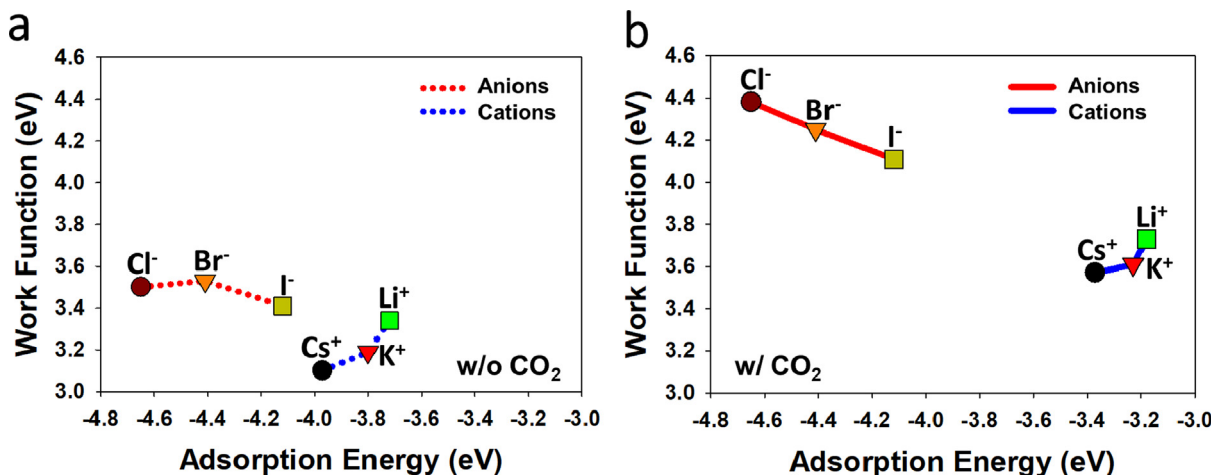
Fig. 3. Calculated adsorption energy and work function (a) before and (b) after CO_2 adsorption on the Bi-2H in the presence of different single type of ions. The clean Bi has a work function of 3.41 eV according to the GGA + D2 method.
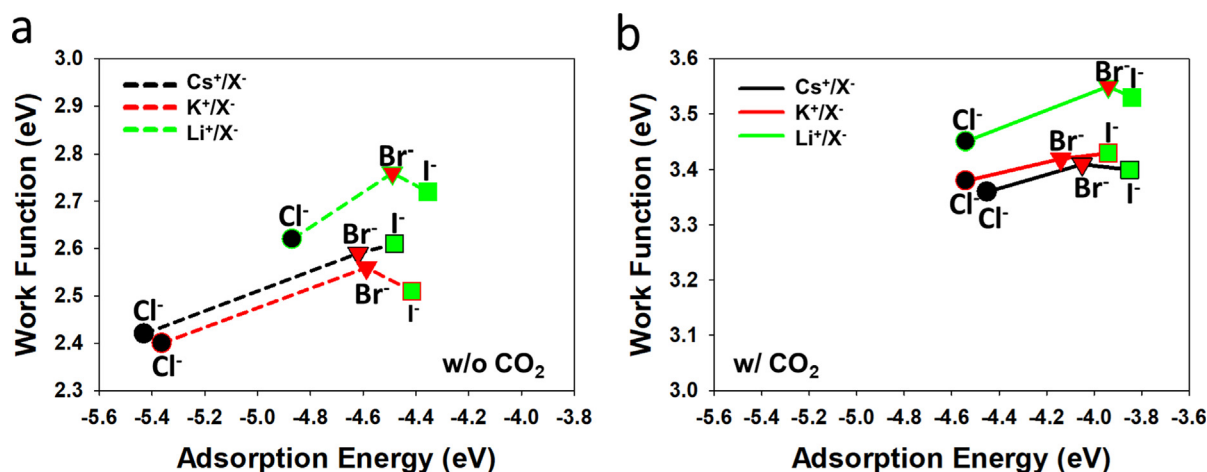
Fig. 4. Comparison of adsorption energy vs. work function (a) in the adsorption of cation (M^+: Cs^+, K^+, and Li^+) and anion (X^-: Cl^-, Br^-, and I^-) pair onto Bi-2H and (b) in the CO_2 adsorption onto Bi-2H pre-adsorbed with M^+/X^- pairs.
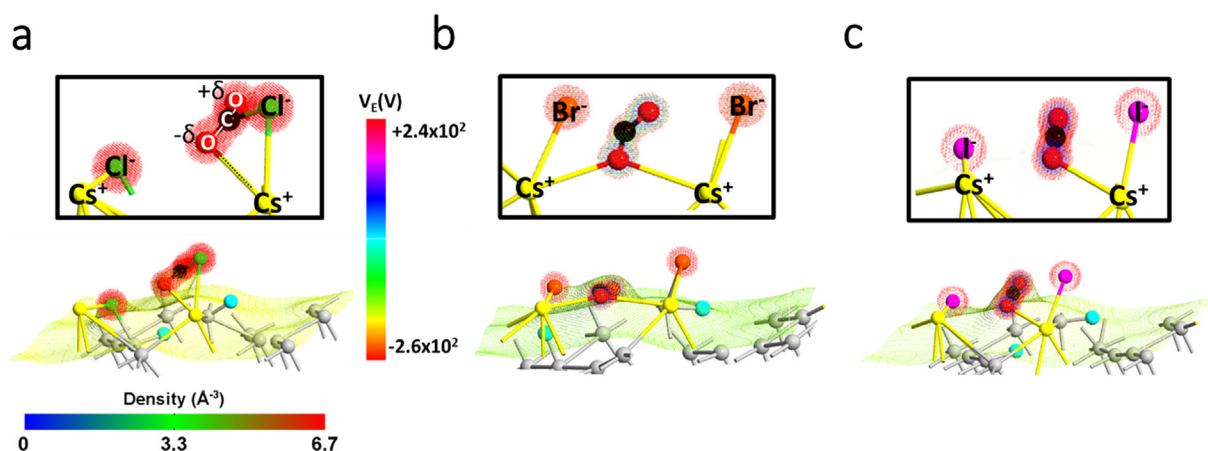
Fig. 5. Combined plots of electron density (A^{-3}) and electrostatic potential (V) of a CO_2 molecule adsorbed on Bi-2H pre-adsorbed with (a) Cs^+/Cl^-, (b) Cs^+/Br^-, and (c) Cs^+/I^-. For comparison, the isovalue for the electrostatic potential isosurface was set at -180 V and the minimum value of electron density was set at 0.65 A^{-3}.

CO_2*) and indirectly in the presence of cations (i.e., Bi → cations → CO_2*). The molecular angle of CO_2* in the oxygen bidentate adsorption increases with increasing anion size (124.1° for Cl^- < 130.2° for Br^- < 172.7° for I^-) (Fig. S1a–c); in contrast, the angle in the oxygen monodentate adsorption decreases with increasing cation size (144.3° for Li^+ < 176.2° for K^+ < 177.8° for Cs^+) (Fig. S1d–f). Considering the three-fold effect of ionic size on CO_2RR (adsorption energy, work function, and molecular angle), the Cs^+ effect is obvious: decreasing the CO_2 adsorption energy and reducing the work function for the electron transfer from the preadsorbed Cs^+ (on Bi atom) to CO_2*. On the other hand, the positive effect of Cl^- (decrease in E_{ads}) should be offset by the effect of the increase in W_f; the overall effect on CO_2RR should be determined by the relative magnitudes of the two.

The E_{ads} values of cation–anion pairs were further calculated. As shown in Fig. 4a, the adsorption energies of M^+/X^- were greater than those of the respective single types of ions (i.e., M^+ or X^-) at Bi (012)-2H surface (e.g., E_{ads} = -3.97, -4.65, and -5.43 eV for Cs^+, Cl^-, and Cs^+/Cl^-, respectively; see Table S1). The large E_{ads} values of the ion pairs indicate that they have more stable and charge-rich states for following CO_2 adsorption. Such the enhanced effect by co-presence of cations and anions was also found for W_f. For example, W_f of Cs^+/Cl^- was estimated to be 2.42 eV, whereas W_f values of Cs^+ and Cl^- were 3.10 and 3.50 eV, respectively. The attraction between M^+ and X^- on the Bi-2H appears to decrease the W_f and facilitate the electron transfer to CO_2*. In addition, the CO_2 adsorption energy with the ion pairs

(> -3.84 eV) was greater than that with one kind of ions (< -3.64 eV) (Fig. 4b). Such a synergistic effect of mixed ions was also observed for the W_f values (< 3.55 eV), which were lower than those with one type of ions (> 3.57 eV). This indicates that the pre-adsorption of the ion pairs provides a better environment for the adsorption and reduction of CO_2 than one type of ions.

The geometrical structures and charge changes of CO_2 adsorbed onto Bi-2H with M^+/X^- pairs were examined (Fig. S2). Although CO_2* was distorted by changes in some molecular angles and O−C−O distances, the optimized CO_2 adsorption configuration was found to be the same as that with the cations (i.e., oxygen monodentate coordination). Such direct bonding of the cations and the bent CO_2 molecule is attributed to ion–dipole interactions. In addition, the net charge obtained by the Bader charge analysis indicates how much charge transfer occurs between the ion and CO_2 molecules on the Bi surface. The net charge of O−C−O in the bent CO_2 molecule is negative, indicating CO_2 activation. On the other hand, negative and positive signs with the adsorbed ions mean that charges are accumulated and depleted, respectively, during CO_2 activation. To examine the reaction activity of CO_2* in the oxygen monodentate, joint plots of the electron density and electrostatic potential were illustrated in a visual manner (Fig. 5). The electron density isosurface plays as a descriptor of electrons at a particular value and indicates that electrons are more concentrated in CO_2* and anions. Among the anions in the presence of Cs^+, the magnitude of electron density for Cl^- was largest followed by Br^- and I^-. Similar results were

observed for K^+/X^- and Li^+/X^- pairs (Fig. S3).

In addition, high electron density was found around the oxygen atoms of CO_2^*. In typical, if CO_2 with a non-dipole moment has a bent molecular structure during adsorption [39], then the positive charge of C atom and the negative charge of the O atom in the bent O−C−O have a dipole moment (Fig. S2). The topography of electrostatic potential further illustrates a three-dimensional contour map that identifies the reactive sites of Bi-2H for electrophilic attack of CO_2. The CO_2 molecule and halide ions encircled by a negative region have charge density leading to electric fields and favors positive charge species such as proton. On the contrary, the positive region has the maximum electronic potential to act as electron donors. This indicates that adsorbed CO_2 species necessarily bind to proton, causing a reduction reaction to transform into C−H products.

3.3. Reaction pathways for HCOOH formation

Based on aforementioned adsorption studies, the electrochemical CO_2RR pathways on Bi-2H with M^+/X^- pairs in aqueous media was simulated while considering the proton-coupled electron (H^+/e^-) transfers in the initial stage followed by the C−H bond formation and/or O−C bond breakage (R1)–(R4).

$$CO_2 \rightarrow CO_2^* \qquad (R1)$$

$$CO_2^* + H^+ + e^- \rightarrow \text{*OCHO (Path-I) or *COOH (Path-II)} \qquad (R2)$$

$$\text{*OCHO (or *COOH)} + H^+ + e^- \rightarrow \text{HCOOH*} \qquad (R3)$$

$$\text{HCOOH*} \rightarrow \text{HCOOH} + * \qquad (R4)$$
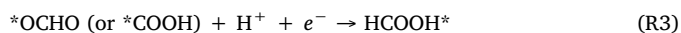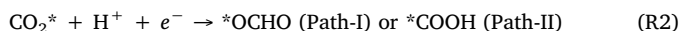
Two reaction intermediates (oxygen-bound *OCHO intermediate and carbon-bound *COOH intermediate) were considered and their free energy diagrams were constructed. Two reaction pathways were examined until reaching the desorption state of final product (HCOOH*) from gas-phase CO_2 adsorption through the *OCHO and *COOH intermediates (Fig. 6). More detailed information about the adsorption configurations of *OCHO, *COOH, and HCOOH* is shown in Fig. S4, S5, and S6, respectively.

Cs^+/X^-: Fig. 6a shows the reaction pathways in the presence of Cs^+/X^-. For the *OCHO-mediated pathway (Path-I), the CO_2 adsorption (R1) with Cl^- was more favorable than those with Br^- and I^-. The same tendency was found for the *COOH-mediated pathway (Path-II). In the following first and second H^+/e^- transfer steps ((R2) and (R3), respectively), the free energies with Br^- and Cl^- were significantly lower than that with I^- in both pathways. However, the *OCHO-mediated pathway was favored over the *COOH for the same anions in the first H^+/e^- transfer step (R1). This indicates the former being a dominant intermediate. In the desorption step (R4), the low free energy of Cl^{-} allows to produce HCOOH more preferentially than Br^- and I^-, suggesting that the presence of Cl^- results in a more favorable pathway to produce HCOOH.

K^+/X^-: Fig. 6b also compares the effects of K^+/X^- on HCOOH formation through the two Paths. In the *OCHO-mediated route (Path-I), Cl^- was found to be the most beneficial in CO_2 adsorption and desorption of HCOOH*. The latter step was endergonic for Br^- and I^-. In the *COOH-mediated route (Path-II), CO_2 adsorption with I^- and desorption of HCOOH* with Cl^- and Br^- were endergonic. Overall, Path-I is favored over Path-II, which is similar to the case of Cs^+/X^-.

Li^+/X^-: The reaction pathway diagram with Li^+/X^- was also compared (Fig. 6c). In the *OCHO-mediated route (Path-I), Cl^- was the most effective in the CO_2 adsorption and yet made the HCOOH* desorption most endergonic. In the Path-II, the CO_2 adsorption step is the most endergonic with Br^- and I^-, whereas the first H^+/e^- transfer step requires a significant energy with Cl^-. Overall, Li^+/X^- favors Path-I slightly over Path-II, like the cases of Cs^+/X^- and K^+/X^-.

As discussed above, the *OCOH-mediated routes require less energy than the *COOH-mediated ones in all the cases of M^+/X^-. Hence the

HCOOH formation should predominantly follow the former route on Bi-2H surface, which is consistent to the other computational mechanism studies on the photocatalytic and electrocatalytic HCOOH production [2,11,39–42]. In the *OCOH-mediated route, cascaded reaction profiles from CO_2^* with overall energies of 0.37 eV and 0.50 eV were obtained with Cs^+/Cl^- and K^+/Cl^- pairs, respectively. This indicates that once CO_2 is adsorbed, then the following reactions proceed spontaneously on the Bi-2H with either Cs^+/Cl^- or K^+/Cl^- pairs. Our recent experimental study found a positive effect of supporting CsCl and KCl electrolytes on the electrocatalytic conversion of CO_2 to HCOOH with porous Bi dendrites [2,11,40], consistent with this computational result.

4. Conclusions

This DFT study revealed that alkali metal cations and halide anions pairs played major roles in determining the reaction pathways of electrochemical CO_2 reduction on the Bi surface. The adsorption of a single type of ions (except for H^+) occurred spontaneously (i.e., $E_{ads} < 0$) with larger adsorption energies for the smaller anions and the larger cations. In the co-presence of the anions and cations, the adsorption energy of cation–anion pairs on hydrated Bi (Bi-2H) became more negative than the cases of the anions alone and the cations alone, particularly when the cation is larger than the paired anion. Such a synergistic effect of the mixed ions was found for the work function values as well. This suggests that the Bi surface adsorbed with the mixed ions are promising for CO_2 adsorption and following interfacial electron transfer. The simulation on the CO_2RR pathways on the Bi-2H surface adsorbed with the mixed ions confirmed this hypothesis. Between the two possible reaction pathways involving *OCHO and *COOH intermediates, the former pathway required less energy than the latter in all types of the cation–anion pairs. This suggests that the selective HCOOH formation on Bi surface proceeds predominantly via the *OCHO intermediates. In this route, cascaded reaction profiles from CO_2^* to HCOOH with overall energies of 0.37 eV and 0.50 eV were obtained with Cs^+/Cl^- and K^+/Cl^- pairs, respectively. Accordingly, once CO_2 is adsorbed, the following reactions proceed spontaneously on the Bi-2H with either Cs^+/Cl^- or K^+/Cl^- pairs. This finding is consistent with recent experimental studies on the positive effect of supporting CsCl and KCl electrolytes on the electrocatalytic conversion of CO_2 to HCOOH with porous Bi dendrites.

CRediT authorship contribution statement

Sun Hee Yoon: Writing - original draft. **Guangxia Piao:** Writing - original draft. **Hyunwoong Park:** Writing - review & editing. **Nimir O. Elbashir:** Writing - review & editing. **Dong Suk Han:** Supervision, Writing - review & editing.

Declaration of Competing Interest

The authors declare that they have no known competing financial interests or personal relationships that could have appeared to influence the work reported in this paper.
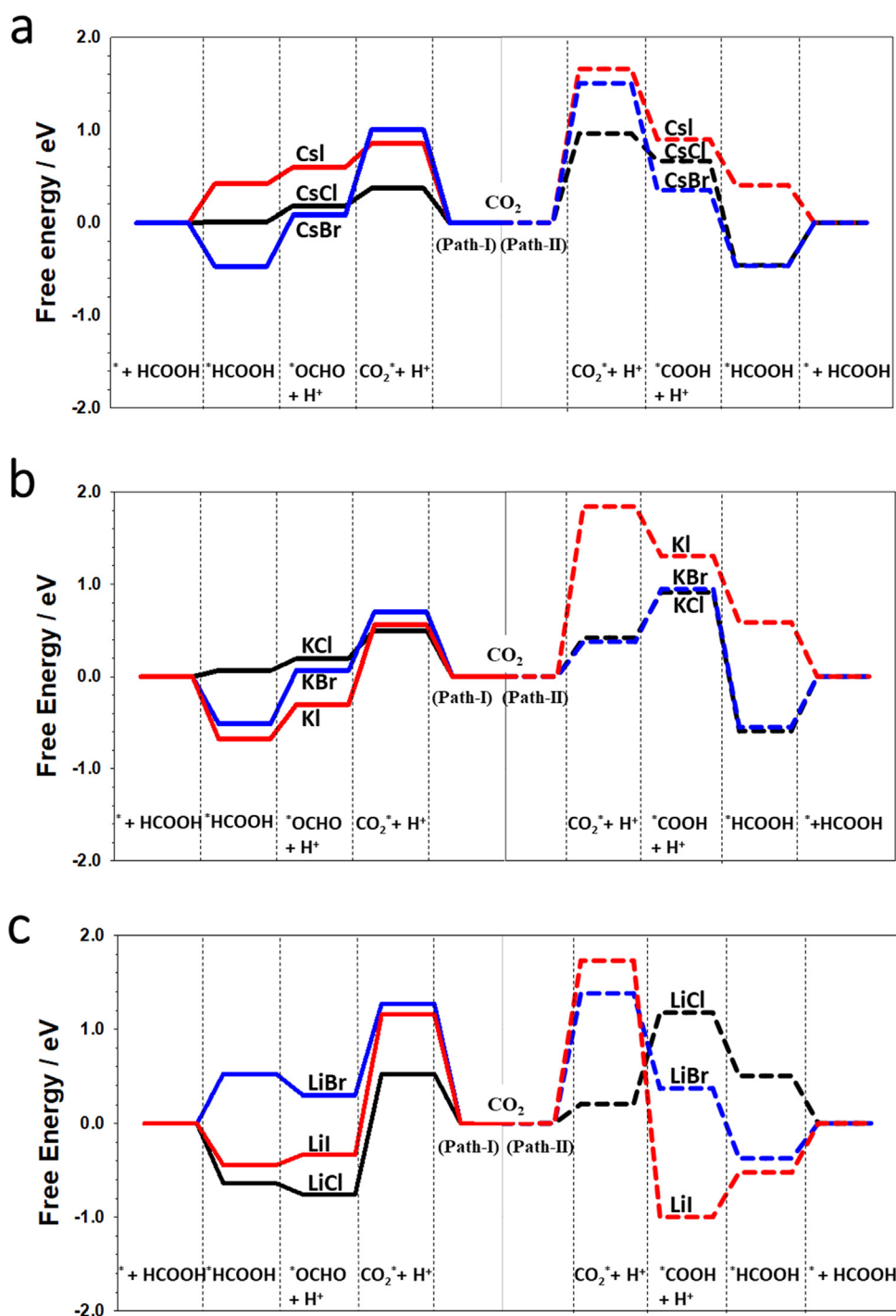
Fig. 6. Comparison of free energy diagrams for reaction energy pathways to form HCOOH via *OCHO and *COOH intermediates on Bi-2H with (a) Cs^+/Cl^-, Cs^+/Br^-, and Cs^+/I^-, (b) K^+/Cl^-, K^+/Br^-, and K^+/I^-, and (c) Li^+/Cl^-, Li^+/Br^-, and Li^+/I^-.

Appendix A. Supplementary material

Supplementary data to this article can be found online at https://doi.org/10.1016/j.apsusc.2020.147459.

References

[1] W. Deng, L. Zhang, L. Li, S. Chen, C. Hu, Z.-J. Zhao, T. Wang, J. Gong, Crucial role of surface hydroxyls on the activity and stability in electrochemical CO₂ reduction, J. Am. Chem. Soc. 141 (2019) 2911–2915.

[2] G. Piao, S.H. Yoon, D.S. Han, H. Park, Ion-enhanced conversion of CO₂ to formate on porous dendrite bismuth electrodes with high efficiency and durability, ChemSusChem 13 (2020) 698–706.

[3] A. Atifi, T.P. Keane, J.L. DiMeglio, R.C. Pupillo, D.R. Mullins, D.A. Lutterman, J. Rosenthal, Insights into the composition and function of a bismuth-based catalyst for reduction of CO₂ to CO, J. Phys. Chem. C 123 (2019) 9087–9095.

[4] S. Ohya, S. Kaneco, T. Katsumata, T. Suzuki, K. Ohta, Electrochemical reduction of CO₂ in methanol with aid of CuO and Cu₂O, Catal. Today 148 (2009) 329–334.

[5] A.R. Paris, A.B. Bocarsly, Mechanistic insights into C2 and C3 product generation using Ni$_3$Al and Ni$_3$Ga electrocatalysts for CO$_2$ reduction, Faraday Discuss. 215 (2019) 1–17.

[6] T. Gao, X. Wen, T. Xie, N. Han, K. Sun, L. Han, H. Wang, Y. Zhang, Y. Kuang, X. Sun, Morphology effects of bismuth catalysts on electroreduction of carbon dioxide into formate, Electrochim. Acta 305 (2019) 388–393.

[7] S.K. Choi, U. Kang, S. Lee, D.J. Ham, S.M. Ji, H. Park, Sn-coupled p-Si nanowire arrays for solar formate production from CO$_2$, Adv. Energy Mater. 4 (2014) 1301614.

[8] S.K. Choi, G. Piao, W. Choi, H. Park, Highly efficient hydrogen production using p-Si wire arrays and NiMoZn heterojunction photocathodes, Appl. Catal. B 217 (2017) 615–621.

[9] S.Y. Choi, C.-D. Kim, D.S. Han, H. Park, Facilitating hole transfer on electrochemically synthesized p-type CuAlO$_2$ films for efficient solar hydrogen production from water, J. Mater. Chem. A 5 (2017) 10165–10172.

[10] N.C. Deb Nath, S.Y. Choi, H.W. Jeong, J.-J. Lee, H. Park, Stand-alone photoconversion of carbon dioxide on copper oxide wire arrays powered by tungsten trioxide/dye-sensitized solar cell dual absorbers, Nano Energy 25 (2016) 51–59.

[11] B.-J. Kim, G. Piao, S. Kim, S.Y. Yang, Y. Park, D.S. Han, H. Shon, M.R. Hoffmann, H. Park, High efficiency solar desalination accompanying electrocatalytic conversions of desalted chloride and captured carbon dioxide, ACS Sust. Chem. Eng. 7 (2019) 15320–15328.

[12] W. Choi, M. Kim, B.J. Kim, Y. Park, D.S. Han, M.R. Hoffmann, H. Park, Electrocatalytic arsenite oxidation in bicarbonate solutions combined with CO$_2$ reduction to formate, Appl. Catal. B-Environ. 265 (2020).

[13] J.L. DiMeglio, J. Rosenthal, Selective conversion of CO$_2$ to CO with high efficiency using an inexpensive bismuth-based electrocatalyst, J. Am. Chem. Soc. 135 (2013) 8798–8801.

[14] J.H. Koh, D.H. Won, T. Eom, N.K. Kim, K.D. Jung, H. Kim, Y.J. Hwang, B.K. Min, Facile CO$_2$ electro-reduction to formate via oxygen bidentate intermediate stabilized by high-index planes of Bi dendrite catalyst, ACS Catal. 7 (2017) 5071–5077.

[15] M.R. Singh, Y. Kwon, Y. Lum, J.W. Ager, A.T. Bell, Hydrolysis of electrolyte cations enhances the electrochemical reduction of CO$_2$ over Ag and Cu, J. Am. Chem. Soc. 138 (2016) 13006–13012.

[16] Y. Yuan, H. You, L. Ricardez-Sandoval, Recent advances on first-principles modeling for the design of materials in CO$_2$ capture technologies, Chin. J. Chem. Eng. 27 (2019) 1554–1565.

[17] F. Quan, M. Xiong, F. Jia, L. Zhang, Efficient electroreduction of CO$_2$ on bulk silver electrode in aqueous solution via the inhibition of hydrogen evolution, Appl. Surf. Sci. 399 (2017) 48–54.

[18] Y.-C. Hsieh, S.D. Senanayake, Y. Zhang, W. Xu, D.E. Polyansky, Effect of chloride anions on the synthesis and enhanced catalytic activity of silver nanocoral electrodes for CO$_2$ electroreduction, ACS Catal. 5 (2015) 5349–5356.

[19] M. Cho, J.T. Song, S. Back, Y. Jung, J. Oh, The role of adsorbed CN and Cl on an Au electrode for electrochemical CO$_2$ reduction, ACS Catal. 8 (2018) 1178–1185.

[20] D. Gao, F. Scholten, B.R. Cuenya, Improved CO$_2$ electroreduction performance on plasma-activated Cu catalysts via electrolyte design: Halide effect, ACS Catal. 7 (2017) 5112–5120.

[21] "ATOMISTIX TOOLKIT version-2019.03", Synopsys QuantumATK (https://www.synopsys.com/silicon/quantumatk.html).

[22] A.S. Varela, W. Ju, T. Reier, P. Strasser, Tuning the catalytic activity and selectivity of Cu for CO$_2$ electroreduction in the presence of halides, ACS Catal. 6 (2016) 2136–2144.

[23] J. Ko, H. Kwon, H. Kang, B.-K. Kim, J.W. Han, Universality in surface mixing rule of

[24] adsorption strength for small adsorbates on binary transition metal alloys, Phys. Chem. Chem. Phys. 17 (2015) 3123–3130.

[24] M. Mavrikakis, P. Stoltze, J.K. Norskov, Making gold less noble, Catal. Lett. 64 (2000) 101–106.

[25] S. Izzaouihda, K. Mahjoubi, H. Abou El Makarim, N. Komiha, D.M. Benoit, Adsorption of imidazole on Au(111) surface: Dispersion corrected density functional study, Appl. Surf. Sci. 383 (2016) 233–239.

[26] F. Zhang, J.D. Gale, B.P. Uberuaga, C.R. Stanek, N.A. Marks, Importance of dispersion in density functional calculations of cesium chloride and its related halides, Phys. Rev. B 88 (2013) 054112.

[27] S.H. Yoon, C. Yu, A. Han, H. Park, N. Elbashir, D.S. Han, Computational characterization of nitrogen-doped carbon nanotube functionalized by Fe adatom and Fe substituent for oxygen reduction reaction, Appl. Surf. Sci. 485 (2019) 342–352.

[28] A.S. Quantumwise, Atomistix Toolkit manual version 2015.1, 2015.

[29] J.K. Nørskov, J. Rossmeisl, A. Logadottir, L. Lindqvist, J.R. Kitchin, T. Bligaard, H. Jónsson, Origin of the overpotential for oxygen reduction at a fuel-cell cathode, J. Phys. Chem. B 108 (2004) 17886–17892.

[30] X.W. Nie, W.J. Luo, M.J. Janik, A. Asthagiri, Reaction mechanisms of CO$_2$ electrochemical reduction on Cu(111) determined with density functional theory, J. Catal. 312 (2014) 108–122.

[31] A.A. Peterson, F. Abild-Pedersen, F. Studt, J. Rossmeisl, J.K. Norskov, How copper catalyzes the electroreduction of carbon dioxide into hydrocarbon fuels, Energy Environ. Sci. 3 (2010) 1311–1315.

[32] B. Ren, J. Li, G. Wen, L. Ricardez−Sandoval, E. Croiset, First-principles based microkinetic modeling of CO$_2$ reduction at the Ni/SDC cathode of a solid oxide electrolysis cell, J. Phys. Chem. C 122 (2018) 21151–21161.

[33] B. Ren, E. Croiset, L. Ricardez-Sandoval, A theoretical study on CO$_2$ electrolysis through synergistic manipulation of Ni/Mn doping and oxygen vacancies in La(Sr) FeO$_3$, J. Catal. 383 (2020) 273–282.

[34] A. Ignaczak, DFT calculations of the interaction of alkali ions with copper and silver, J. Electroanal. Chem. 495 (2001) 160–168.

[35] K.P. Jensen, W.L. Jorgensen, Halide, ammonium, and alkali metal ion parameters for modeling aqueous solutions, J. Chem. Theory Comput. 2 (2006) 1499–1509.

[36] G. Tóth, E. Spohr, K. Heinzinger, SCF calculations of the interactions of alkali and halide ions with the mercury surface, Chem. Phys. 200 (1995) 347–355.

[37] X. Shen, Y. Pan, B. Liu, J. Yang, J. Zeng, Z. Peng, More accurate depiction of adsorption energy on transition metals using work function as one additional descriptor, Phys. Chem. Chem. Phys. 19 (2017) 12628–12632.

[38] E. Olsson, G. Chai, M. Dove, Q. Cai, Adsorption and migration of alkali metals (Li, Na, and K) on pristine and defective graphene surfaces, Nanoscale 11 (2019) 5274–5284.

[39] S.H. Yoon, U. Kang, H. Park, A. Abdel-Wahab, D.S. Han, Computational density functional theory study on the selective conversion of CO$_2$ to formate on homogeneously and heterogeneously mixed CuFeO$_2$ and CuO surfaces, Catal. Today 335 (2019) 345–353.

[40] U. Kang, S.H. Yoon, D.S. Han, H. Park, Synthesis of aliphatic acids from CO$_2$ and water at efficiencies close to the photosynthesis limit using mixed copper and iron oxide films, ACS Energy Lett. 4 (2019) 2075–2080.

[41] U. Kang, S.K. Choi, D.J. Ham, S.M. Ji, W. Choi, D.S. Han, A. Abdel-Wahabe, H. Park, Photosynthesis of formate from CO$_2$ and water at 1% energy efficiency via copper iron oxide catalysis, Energy Environ. Sci. 8 (2015) 2638–2643.

[42] U. Kang, H. Park, A facile synthesis of CuFeO$_2$ and CuO composite photocatalyst films for production of liquid formate from CO$_2$ and water over a month, J. Mater. Chem. A 5 (2017) 2123–2131.